Available online at www.sciencedirect.com
SCIENCE DIRECT®
Acta Materialia 52 (2004) 3459–3466
Acta MATERIALIA
www.actamat-journals.com

Strength of silicon, sapphire and glass in the subthreshold flaw region

Yeon-Gil Jung [1], Antonia Pajares [2], Rajat Banerjee [3], Brian R. Lawn *

Materials Science and Engineering Laboratory, National Institute of Standards and Technology, Bldg. 223, Rm. B309, 100 Bureau Drive, Gaithersburg, MD 10899-8500, USA

Received 23 December 2003; accepted 26 March 2004
Available online 7 May 2004

Abstract

Strength properties are determined for monocrystalline silicon and sapphire and for soda-lime glass plates containing subthreshold flaws, i.e. flaws without detectable microcracks. Nanoindentations covering a wide range of loads are used to introduce flaws of predetermined sizes into highly polished or etched surfaces, to enable systematic study of the transition from the postthreshold to subthreshold regions. Strengths of the indented plates are measured using a simple bilayer test configuration in which the plates are bonded – indentations downward – onto a polycarbonate support base and loaded centrally at their top surfaces to failure. Failure occurs from flaw sites over the entire range of diminishing loads, up to a strength cutoff at >2 GPa associated with natural surface flaws. In none of the materials do the postthreshold strength/indentation-load data extrapolate unconditionally into the subthreshold region. However, whereas the glass data show an abrupt increase in strength at the threshold, the silicon and sapphire data show only a slight discontinuity in slope. A simple model for subthreshold flaws, based on the critical conditions to initiate radial cracking from embryonic shear faults within the contact damage sites, accounts for the main size trends in the data. The disparities between the glass and crystalline responses are attributed to differences in the precursor shear fault geometries. General applicability of the scaling concepts to a broad range of alternative flaw types, e.g. associated with microstructural defects, is discussed.
Published by Elsevier Ltd on behalf of Acta Materialia Inc.

Keywords: Sapphire; Silicon; Glass; Strength; Nanoindentation; Subthreshold flaws

1. Introduction

With the continuing miniaturization of MEMS, NEMS, sensors and actuators, bioengineering devices, etc., questions inevitably arise as to any changes in fundamental material response as characteristic dimensions diminish into the small-scale region. These dimensions include specimen size, interlayer thickness, microstructural scale, and inter-component contact dimensions [1,2]. From the standpoint of inherently brittle materials, most pressing is how material strength may change as this region is entered. How valid is it to extrapolate macroscopic fracture and deformation laws unconditionally downward? – and, if such extrapolations prove not to remain valid, what are the new, nanomechanics-based laws that govern behavior in the small-scale region?

One of the defining size scales in brittle behavior is that of the critical flaw responsible for fracture under applied stress. The basic nature of flaws in the submicrometer region and associated strength properties remain obscure. An illustrative example is that of optical glass fibers, which in their pristine state can achieve strengths approaching 10 GPa [3]. However, surface contact with a single μm-scale atmospheric particle can

* Corresponding author. Tel.: +1-301-975-5775; fax: +1-301-975-5012.
E-mail address: brian.lawn@nist.gov (B.R. Lawn).
[1] On leave from Department of Ceramic Science and Engineering, Changwon National University, Sarim-dong 9, Changwon, Kyung-Nam, Republic of Korea.
[2] On leave from Departamento de Física, Facultad de Ciencias, Universidad de Extremadura, 06071 Badajoz, Spain.
[3] On leave from Optical Glass Division, Central Glass and Ceramic Research Institute, 196 Raja S.C. Mullick Road, Jadavpur, Kolkata 700032, West Bengal, India.

1359-6454/$30.00 Published by Elsevier Ltd on behalf of Acta Materialia Inc.
doi:10.1016/j.actamat.2004.03.043

reduce the fiber strength by over an order of magnitude. Flaws in this region may not have the nature of classical Griffith microcracks, but may rather take the form of embryonic defects with intensely concentrated residual stress fields [4,5]. Such defects can arise from extrinsic surface contacts from dust particulates, from inclusions in the bulk material [6], or from local contacts with moving components in a micromechanical (e.g., MEMS) device. These "subthreshold" defects do not develop into true microcracks until some characteristic flaw dimension or subsequent applied stress level is exceeded: in the subthreshold region fracture is initiation-controlled, whereas in the postthreshold region fracture is propagation-controlled.

The present paper addresses this issue of flaw size in highly brittle materials, using sharp indentations to introduce controlled subthreshold flaws. Such indentations may be expected to simulate the kind of microcontacts that occur in real small-scale structures. Although the loads can be minute, <1 mN in extreme cases, the contact forces are concentrated and so can deliver high local stresses, sufficient to induce strength-degrading flaws. Previous indentation studies in silicate glasses and crystalline ceramic materials have demonstrated contact damage zones beneath sharp indenters to consist of arrays of constrained discrete shear or slip faults, activated at stresses close to the cohesive strength of the material [7–12]. Well-defined radial cracks initiate from the faults, either spontaneously at sufficiently high indentation loads (postthreshold flaws) or subsequently under the action of applied tensile stresses (subthreshold flaws), thereby degrading the strength properties [13–16]. Recent observations of nanoindentation damage sites in semiconductor single crystals have revealed insight into the fundamental precursor slip and subsequent fracture processes [17–19].

The specific goal of this paper is to determine the strength of select brittle materials containing contact flaws made with sharp nanoindenters, as a function of indentation load or equivalent flaw size. The materials considered are single-crystal silicon and sapphire with polished surfaces, chosen for both their widespread use as model brittle materials and their potential applications in small-scale device systems. Preliminary data for silicon have already been reported [16], but are here extended in data range. Soda-lime glass is also included as a well-documented comparative base material. A fracture mechanics description, building on earlier fracture mechanics models [5,13,20–22] but here highly simplified, is used to account for the basic elements of crack initiation and attendant strength degradation from precursor shear faults. Particular attention is paid to properties in the indentation crack threshold region, where the associated strength properties may be expected to undergo a fundamental transition. Implications concerning the generic behavior of stress-concentrating, small-scale flaws will be discussed.

2. Experimental procedure

Silicon wafers (University Wafer, South Boston, MA) with (1 1 1) surfaces and sapphire wafers (Valley Design Corp., Santa Cruz, CA) with $(10\bar{1}2)$ surfaces were cut into plates 25 mm × 25 mm × 1 mm. The wafers were procured in a polished state with <1 nm surface roughness. Soda-lime glass plates were cut to similar dimensions from microscope slides (Fisher Scientific, Pittsburgh, PA) and surface-etched (10 vol% HF for 9 min) to remove handling defects. Care was taken to protect the finished surfaces from any spurious damage throughout the handling process.

Controlled flaws were introduced into the plate top centers using diamond indenters: for loads in the range 200 down to 2 N, a microindenter (Zwick 3212, Zwick USA, Kennesaw, Georgia) with Vickers tip; for loads in the range 10 N down to 1 mN, a nanoindenter (Nanoindenter XP, MTS Systems Corp., Oakridge, TN) with Berkovich tip (tip radius <100 nm). (The Vickers and Berkovich indenters are designed to give equivalent contact areas at any given load.) The load ranges for each indenter allow for some data overlap. All indentations were made in air. The indenter axes relative to the crystal orientations were random. Load–displacement (P–h) functions were recorded, and hardness H and modulus E calculated, for each Berkovich nanoindentation [23]. The indentation sites were examined for cracking using an atomic force microscope (AFM – Digital Instruments Nanoscope IIIa, Veeco Metrology, Santa Barbara, CA) using a gold-coated silicon tip in contact mode. Toughness T was evaluated from radial crack lengths at Vickers indentations in the high load region using a standard formulation by Anstis et al. [24].

A simple bilayer test was used to measure the strengths of the indented plates, Fig. 1 [25,26]. The plates were inverted and the indentation surface then bonded with a thin layer of epoxy (~10 μm) onto a polycarbonate base 12.5 mm thick. Some plates were

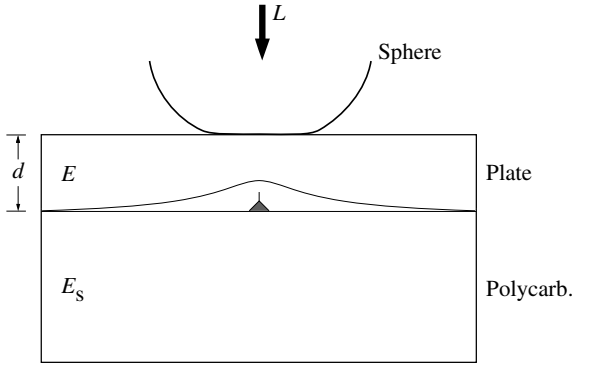

Fig. 1. Bilayer test configuration, with indentation placed at center of plate undersurface and sphere applied at top surface. Bell-shaped curve indicates tensile stress distribution on plate undersurface.

bonded without preindentation so as to determine strengths of non-indented surfaces. The bilayers were then placed onto the specimen stage of a mechanical testing machine (Instron 8500, Instron Corp., Boston, MA) and positioned with the indentation sites aligned along the load axis. This alignment was facilitated using a camera system with a 45° mirror located immediately below a small hole in the stage [25]. A tungsten carbide spherical indenter of radius 3.18 mm was then used to load the bilayer specimens at the plate top surface. In the bilayer specimen configuration the brittle coating layer flexes on the compliant polycarbonate support base, placing the indentation site at the coating undersurface in tension. An advantage of the bilayer configuration is that the tensile stress at the plate underface is concentrated in a central area of radius approximately one plate thickness [27], thus minimizing premature failures from occasional larger defects, edge flaws and specimen supports. In situ camera observations during testing enabled direct confirmation that failure initiated from an indentation flaw. Strengths were calculated using the bilayer relation $S = (L/Bd^2)\log(E/E_s)$, where L is critical the load, d is the plate thickness, E is the modulus of the upper plate and $E_s = 3.25$ GPa the modulus of the polycarbonate substrate, and $B = 1.35$ [28]. Strengths evaluated from this relation may be expected to provide reliable estimates for small (e.g. subthreshold) flaws, where the issue of stress gradients over the flaw length does not arise [29].

3. Theoretical model

3.1. Subthreshold flaws

In this section we present a fracture mechanics analysis for the initiation of radial cracks from quasiplastic damage zones beneath sharp indenters, building on earlier models [5,13,20–22] but with simplifications to enable derivation of basic, explicit relations.

Consider the indentation at load P and characteristic contact radius a or depth h, Fig. 2. The damage zone consists of shear or slip faults whose dimensions are confined within the immediate contact zone [2,11,12]. These faults act as effective sources for initiation of radial cracks. Once initiated, the cracks extend around the contact zone and complete themselves in a half-penny configuration of radius c with characteristic radial traces on the top surface [30]. The main simplification in the present analysis is to treat the critical shear faults as "equivalent" mode I cracks of size $c \approx a$. In this description, the contact radius a may be considered as a measure of the flaw size. The observation of a permanent impression indicates the existence of a residual stress field about the indentation site, the intensity of which scales with the mean contact pressure or hardness H [22,30,31].

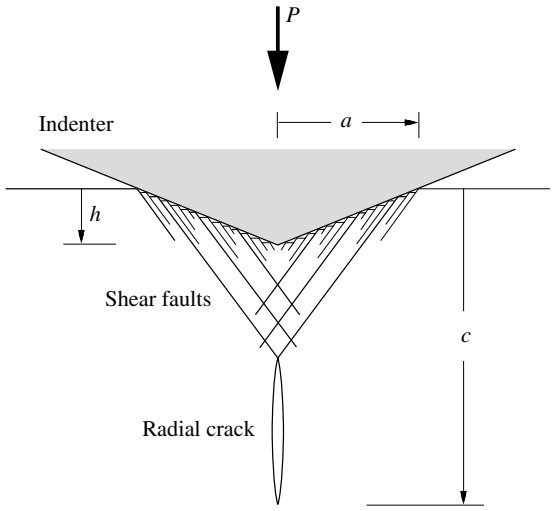

Fig. 2. Schematic showing shear fault formation within hardness quasiplastic zone and subsequent radial crack initiation beneath a sharp indenter.

The stress-intensity factor for the equivalent source crack subjected to a subsequent applied flexural stress σ then has the generic form

$$K = K_R + K_A = \kappa H c^{1/2} + \lambda \sigma c^{1/2}, \tag{1}$$

where κ and λ are crack-geometry coefficients. The source crack at $c = a$ becomes unstable and propagates into a full radial crack at $K = T$ (single-valued toughness, K_{IC}), $\sigma = S$, defining the strength

$$S = (1/\lambda)[T/a^{1/2} - \kappa H]. \tag{2}$$

The strength can equally well be expressed in terms of load P. Defining hardness as the mean contact pressure [32]

$$H = P/\alpha a^2 \tag{3}$$

enables us to rewrite Eq. (2) as

$$S = (1/\lambda)[(\alpha H/P)^{1/4} T - \kappa H] \tag{4}$$

with $\alpha = 3^{3/2}/4$ for Berkovich and $\alpha = 2$ for Vickers indenters ($\alpha =$ indent center-to-corner dimension). It is implicit in Eq. (4) that the hardness remains constant over the load range.

It will be observed that both toughness T and hardness H appear in Eqs. (2) and (4): T determines the condition for crack extension and H determines the magnitude of the residual stress field. The limiting condition $S = 0$ defines threshold contact sizes and loads for spontaneous radial cracking [13,20]:

$$a_* = (T/\kappa H)^2, \tag{5a}$$

$$P_* = 2T^4/\kappa^4 H^3. \tag{5b}$$

3.2. Postthreshold flaws

At $a > a_*$, $P > P_*$, radial crack initiation from the indentation site is spontaneous, defining the postthreshold region. The mechanics of fracture from specimens containing fully developed radial cracks is well documented [30,31,33,34], so we present only the essential results here. In analogy to Eq. (1), the stress-intensity factor for cracks in this region has the form

$$K = K_R + K_A = \chi P/c^{3/2} + \psi\sigma c^{1/2} \tag{6}$$

with χ and ψ crack geometry coefficients. In this case, the radial crack first propagates stably at $K = T$ to $c = c_M$ under the action of the combined residual and applied stress fields prior to failure, defining the strength $\sigma = \sigma_M = S$,

$$S = (3T/4\psi)(T/4\chi P)^{1/3} = \beta(T^4/P)^{1/3}, \tag{7}$$

where $\beta = (3/4\psi)(1/4\chi)^{1/3}$.

Toughness T is thus the primary strength-determining material property in the postthreshold region. Strictly, $\chi \sim (E/H)^{1/2}$ in Eq. (6) [31], but this corresponds to a very weak $(E/H)^{1/6}$ term in the strength relation equation (7), so we ignore any modulus/hardness variation here.

4. Results and analysis

Fig. 3 shows AFM images of nanoindentations in soda-lime glass, silicon (1 1 1) and sapphire $(10\bar{1}2)$, in the immediate subthreshold and postthreshold regions. The images – representing derivatives of surface topography for edge enhancement – reveal well-defined hardness impressions with apparently smooth surfaces within. As we shall argue in Section 5, the smoothness of the indentation surfaces belies the presence of intense damage below. The images in Fig. 3 reveal the existence of cracking thresholds, with radial cracks clearly visible at the higher loads but completely suppressed at the lower loads. Considerable variation was found in the threshold loads for each material, especially for glass, consistent with observations in previous studies [11].

Values of hardness H, modulus E and toughness T shown in Table 1 for the brittle test materials are means and SD of a minimum 25 tests, calculated from the indentation measurements: for H, a combination of evaluations from load–displacement data for the instrumented Berkovich nanoindentations plus direct Vickers impression measurements using Eq. (3); for E, solely from the Berkovich load–displacement data; and for T, from well-developed cracks at Vickers indentations at load $P = 10$ N. The E and H values showed little systematic variation over the load range covered in our experiments, although they are somewhat higher than typically quoted for bulk materials in the literature.

Figs. 4–6 are plots of strength S versus indentation load P (lower axis) or "equivalent dimension" a from Eq. (3) (upper axis) for glass, silicon (1 1 1) and sapphire $(10\bar{1}2)$. Silicon (1 0 0) data, previously reported elsewhere [16], are excluded from Fig. 5 to avoid excessive data overlap – in any case, those data show the same trend as silicon (1 1 1), with only a small (20–30%) upward shift along the strength axis. Symbols are indi-

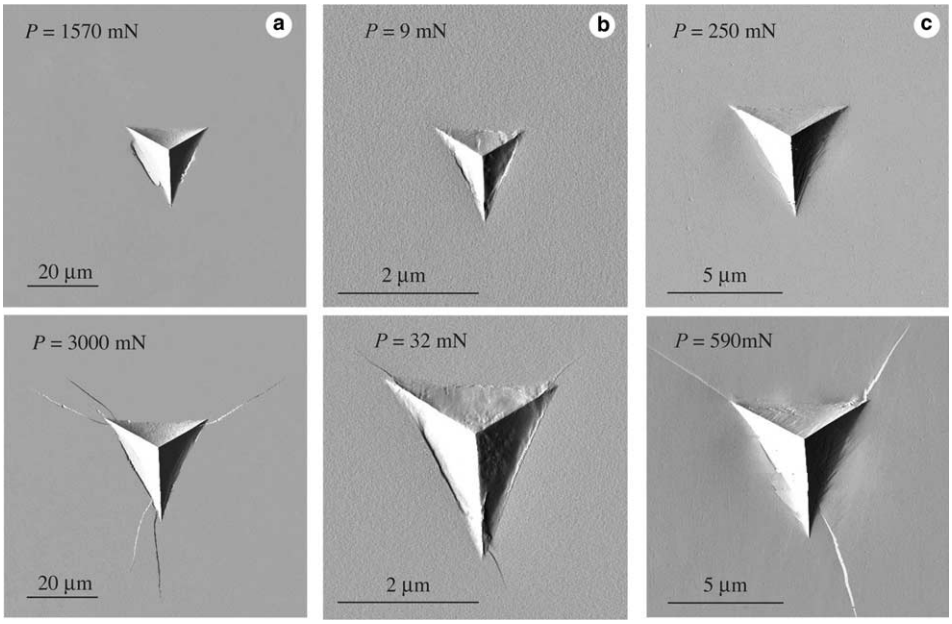

Fig. 3. AFM images of Berkovich nanoindentations in (a) soda-lime glass, (b) silicon (1 1 1) and (c) sapphire $(10\bar{1}2)$. The two indentations for each material represent loads immediately on either side of the radial cracking threshold.

Table 1
Parameters for materials in this study

Material	E (GPa)	H (GPa)	T (MPa m $^{1/2}$)	λ	κ	β
Soda-lime glass	64 ± 4	5.9 ± 0.5	0.70 ± 0.1	0.27	0.015	2.00
Silicon (1 1 1)	200 ± 10	13.5 ± 1	0.9 ± 0.2	0.45	0.068	1.25
Sapphire $(10\bar{1}2)$	470 ± 25	30 ± 3	2.75 ± 0.0	0.55	0.055	1.25

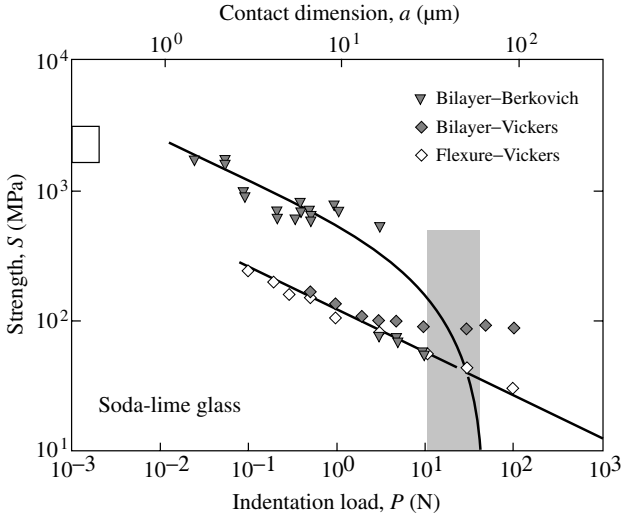

Fig. 4. Strength S of soda-lime glass plates as function of indentation load P (lower axis) or contact dimension a (upper axis). Solid curves are data fits. Vertical band represents cracking threshold range (inert conditions). Vickers–flexure data are from a previous study on optical glass fibers (broken in dry N_2 gas) [15].

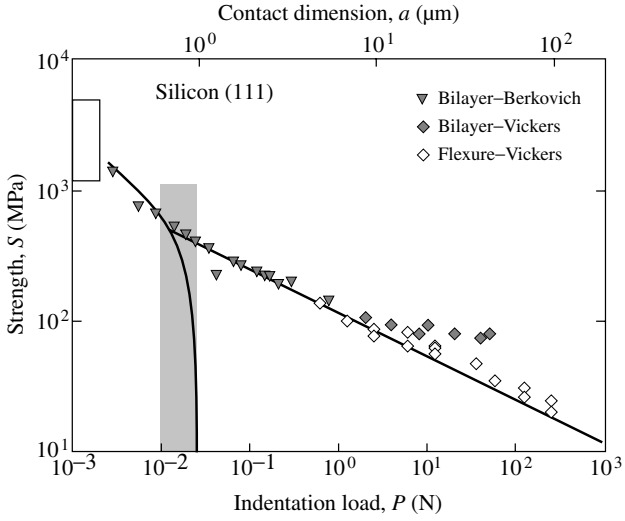

Fig. 5. Same as Fig. 4, but for silicon (1 1 1). Vickers–flexure data are from a previous study on silicon (1 1 1) bars [35].

vidual data points: triangles represent failures from Berkovich indentations, diamonds failures from Vickers indentations; filled symbols represent current bilayer test data, unfilled symbols flexure data from earlier studies

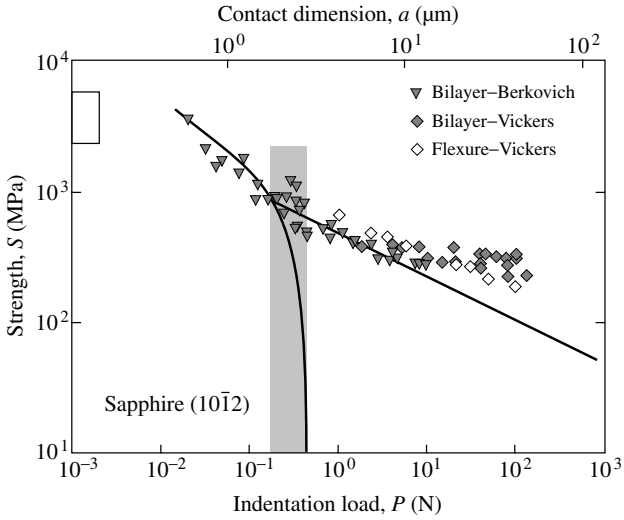

Fig. 6. Same as Fig. 4, but for sapphire $(10\bar{1}2)$ Vickers–flexure data are from a previous study on sapphire rods (broken in air) (data from R.F. Cook, quoted in [34]).

on Vickers-indented bars or disks [15,34,35]. Open boxes on the left axis are SD limits for failures from natural flaws (including failures away from indentation sites in low-load Berkovich specimens), providing an upper cutoff at ~2–4 GPa for the indentation-strength data. Vertical grey bands indicate observed bounds for the threshold cracking loads P_*, above which cracks are always present and below which cracks are never present. The threshold in glass is strongly sensitive to such variable factors as contact duration and relative humidity in the atmosphere [11,29,36,37], so for the purpose of data fitting (see below) the vertical band shown is for a separate series of relatively fast (15 s) Vickers indentation tests in "inert" dry N_2 environment. Where common bilayer and flexure test data are available there is overlap within the scatter in the all-important subthreshold and immediate postthreshold regions, where the flaw sizes c remain small relative to plate thickness d. There is some tendency for the bilayer data to deviate upward relative to the flexure data in the upper postthreshold region $P \gg P_*$, attributable principally to the increasingly constraining effects of tensile stress gradients as c approaches d but also to intrusion of the bonding epoxy into the radial cracks at the interlayer interface [29,38,39]. In the lower subthreshold region, indentation penetration depths ($\sim a/7$) approach the

indenter tip radius ~100 nm used in our experiments (suggesting that extension of the data range to even smaller contact loads could be problematic). Notwithstanding these cutoffs and deviations, transitions in the strength characteristics are evident in all three materials, although the nature of the transition does not appear to be universal. Whereas in glass the strength shows an abrupt increase on traversing the threshold, with considerable data overlap along the load axis, in silicon and sapphire the transition is smooth, with only slight discontinuity in slope.

The solid lines in Figs. 4–6 are theoretical fits to the data, adjusting coefficients in the appropriate strength relations: Eq. (4) in the region $P < P_*$, including only data representing failures from subthreshold indentation sites – i.e. excluding failures from natural flaws – and requiring that the curve intersect the P axis within the observed threshold range; Eq. (7) in the region $P > P_*$, including only bilayer data in the immediate postthreshold region – i.e. excluding bilayer data where deviations from $P^{-1/3}$ flexure data become apparent. In the case of silicon, the subthreshold region is not so well defined by the data points, because of the extremely low value of P_*. Values of the adjusted coefficients are included in Table 1. A near-common set of coefficients adequately fits the postthreshold data for silicon and sapphire, but again not for glass, implying some basic differences in the flaw geometries in the two material classes.

5. Discussion

Strength characteristics have been determined for three classical brittle materials – soda-lime glass, silicon and sapphire – using nanoindentations to introduce small-scale flaws down into the subthreshold region. The indentation flaws have the nature of precursor damage zones containing slip or shear faults: subthreshold flaws are readily distinguished from their postthreshold counterparts by the absence of visible radial cracks at the indentation corners. Strength values in the subthreshold region are higher than would be predicted from extrapolation of data from the postthreshold region, more so in the case of glass than in the crystalline materials. Subthreshold flaws nevertheless still provide preferential sites for failure in subsequent tensile loading.

A fracture mechanics model, simplified from earlier descriptions, accounts for the main features in the strength dependence on flaw size. The postthreshold region is based on propagation from well-developed radial cracks, the subthreshold region on initiation of radial cracks from precursor shear faults. Actually, the analysis predicts another intermediate region between the loads at which the subthreshold and postthreshold curves cross each other and where the subthreshold curve intersects the $S = 0$ axis. In this region the radial crack first initiates in the applied tensile field, arrests, and propagates stably before failure. However, as seen in Figs. 4–6, this region occupies a narrow window along the P axis and the indentations are very small, so any such activated pop-in would be difficult to capture optically.

For the sake of comparison, it is useful to plot the fitted S–P curves for the three materials onto a master diagram. Fig. 7 shows such a plot, with the curves extrapolated beyond the data range into the nanoscale flaw, ultra-high strength region. It is interesting to note how the material ranking changes in the different flaw-size regions. Although glass has the lowest strength in the postthreshold region, because of its inferior toughness, silicon has the lowest strength in the subthreshold region, because of its very low threshold. Also of interest is the reduced superiority of the much tougher sapphire relative to glass in the subthreshold region. The crystalline materials are especially brittle and susceptible to crack initiation from the most minute precursor damage.

The question remains as to why the postthreshold/subthreshold transition is smooth in silicon and sapphire but abrupt in glass. This question has been addressed in earlier studies. In Fig. 4 for glass, the postthreshold data extend to loads well to the left of the crossover between the fitted postthreshold and subthreshold curves. It is argued that such pseudo-subthreshold data actually represent subthreshold flaws that have popped in during or even after unloading of the indenter [5,36]. The persistent action of the residual stress field around indentation sites, in conjunction with the intrusion of moisture into shear-fault source-cracks, causes delayed

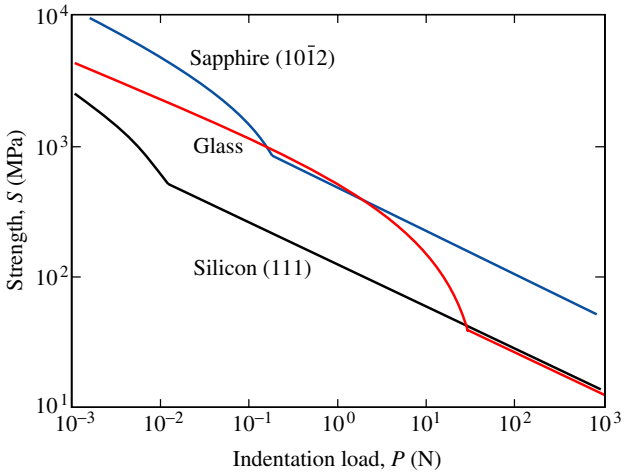

Fig. 7. Composite S–P plot of fitted curves for soda-lime glass, silicon and sapphire in Figs. 4–6. Note crossover in curves, indicating how relative strengths for different materials can switch in postthreshold and subthreshold regions.

radial crack pop-in [11], thereby extending the post-threshold region down toward 100 mN in Fig. 4. Hence the apparent abrupt strength discontinuity in Fig. 4. The somewhat erratic delayed pop-in in glass [11] accounts for the considerable postthreshold/subthreshold data overlap in this figure. Analogous discontinuities are not evident in silicon or sapphire, which are relatively immune or at least insensitive to delayed pop-in from slow crack growth effects.

Another distinction between the glassy and crystalline materials is the disparity in values of the subthreshold parameters λ and κ in Table 1. Such disparity indicates departure from the notion of geometrical similitude implicit in the fracture mechanics model in Section 3.1 – the assumption of shear faults as "equivalent" in-plane mode I source-cracks is simplistic. In all of the materials considered, the plastic deformation occurs at stress levels close to the cohesive strength (typically, $H/E > 0.05$), so that shear faults propagate abruptly and discretely as depicted in Fig. 2 [2]. However, the shear fault configurations in the glassy and crystalline solids are quite different: in the glasses, the faults form on curved surfaces of maximum shear stress trajectories [7,8,11]; in monocrystalline solids, they form preferentially on weak crystallographic slip planes [12,17–19,40–42]. Apparently, the additional constraints imposed by the crystallography favor higher stress concentrations at intersecting shear faults, making it easier to initiate radial cracks. Indenters with much sharper angles than the Berkovich and Vickers used here (e.g. cube corner) can profoundly depress threshold loads [43], attesting to some role of geometry in the crack initiation process.

Although the present study has focused on indentation flaws, we would assert a certain generality in the conclusions. Threshold behavior is common to a wide range of defects. Microcracks analogous to radial cracks are known to initiate from stress concentrations at or around grain boundaries in polycrystals or included particulates (or second phases) in matrix materials above some critical grain dimension, dependent on several material mismatch parameters (e.g. modulus or thermal expansion). Threshold size effects in fracture come about as a result of different scaling dependencies of strain and surface energy terms [34]: strain energy associated with the volume of material scales with (grain dimension)^3, whereas surface energy associated with the formation of crack area scales with (grain dimension)^2. Threshold behavior is expected to be the rule rather than the exception.

Finally, mention may be made of the potential of nanoindentations to investigate how the strength properties of certain brittle materials might be modified by the deposition of thin films – oxide films on silicon, ion implantation, etc. The fracture and damage properties of such materials are expected to be increasingly influenced by the film properties in the high-strength, sub-threshold region, where flaws may be wholly contained within the film thickness.

Acknowledgements

The authors thank Douglas Smith for assistance with the nanoindentation experiments, and Yan Deng and Bryan Huey with the AFM micrographs. This work was sponsored by NIST internal funds; by a grant to Yeon-Gil Jung from the Korea Science and Engineering Foundation (KOSEF Grant KRF-2003-013-D00055); and by a grant to Antonia Pajares from the Junta de Extremadura-Consejeria de Educacion Ciencia y Tecnologia y el Fondo Social Europeo, Spain (Grant IPR00A084) and Secretaria de Estado de Educacion y Universidades, Spain.

References

[1] Arzt E. Acta Mater 1998;16:5611.
[2] Lawn BR. J Mater Res 2004;19:22.
[3] Maurer RD. In: Kurkjian CR, editor. Strength of inorganic glass. New York: Plenum Press; 1985. p. 291.
[4] Lawn BR. J Am Ceram Soc 1983;66:83.
[5] Lin B, Matthewson MJ. Philos Mag A 1996;74:1235.
[6] Swain MV. J Mater Sci 1981;16:151.
[7] Swain MV, Hagan JT. J Phys D 1976;9:2201.
[8] Hagan JT. J Mater Sci 1979;14:2975.
[9] Hagan JT. J Mater Sci 1980;15:1417.
[10] Zwagg Svd, Hagan JT, Field JE. J Mater Sci 1980;15:2965.
[11] Lawn BR, Dabbs TP, Fairbanks CJ. J Mater Sci 1983;18:2785.
[12] Chan HM, Lawn BR. J Am Ceram Soc 1988;71:29.
[13] Lawn BR, Evans AG. J Mater Sci 1977;12:2195.
[14] Dabbs TP, Marshall DB, Lawn BR. J Am Ceram Soc 1980;63:224.
[15] Dabbs TP, Lawn BR. J Am Ceram Soc 1985;68:563.
[16] Pajares A, Chumakov M, Lawn BR. J Mater Res 2004;19:657.
[17] Bradby JG, Williams JS, Wong-Leung J, Swain MV, Munroe P. J Mater Res 2001;16:1500.
[18] Bradby JG, Williams JS, Wong-Leung J, Kucheyev SO, Swain MV, Munroe P. Philos Mag A 2002;82:1931.
[19] Zarudi I, Zhang LC, Swain MV. J Mater Res 2003;18:758.
[20] Lawn BR, Marshall DB. J Am Ceram Soc 1979;62:347.
[21] Jakus K, Ritter JE, Choi SR, Lardner T, Lawn BR. J Non-Cryst Solids 1988;102:82.
[22] Lathabai S, Rödel J, Lawn BR, Dabbs TP. J Mater Sci 1991;26:2157.
[23] Oliver WC, Pharr GM. J Mater Res 1992;7:1564.
[24] Anstis GR, Chantikul P, Marshall DB, Lawn BR. J Am Ceram Soc 1981;64:533.
[25] Chai H, Lawn BR, Wuttiphan S. J Mater Res 1999;14:3805.
[26] Rhee Y-W, Kim H-W, Deng Y, Lawn BR. J Am Ceram Soc 2001;84:1066.
[27] Miranda P, Pajares A, Guiberteau F, Cumbrera FL, Lawn BR. Acta Mater 2001;49:3719.
[28] Miranda P, Pajares A, Guiberteau F, Deng Y, Lawn BR. Acta Mater 2003;51:4347.
[29] Kim H-W, Deng Y, Miranda P, Pajares A, Kim DK, Kim H-E, et al. J Am Ceram Soc 2001;84:2377.
[30] Marshall DB, Lawn BR. J Mater Sci 1979;14:2001.

[31] Lawn BR, Evans AG, Marshall DB. J Am Ceram Soc 1980;63:574.
[32] Tabor D. Hardness of metals. Oxford: Clarendon Press; 1951.
[33] Marshall DB, Lawn BR, Chantikul P. J Mater Sci 1979;14:2225.
[34] Lawn BR. Fracture of brittle solids. 2nd ed. Cambridge: Cambridge University Press; 1993 [chapter 8].
[35] Lawn BR, Marshall DB, Chantikul P. J Mater Sci 1981;16:1769.
[36] Lathabai S, Rödel J, Lawn BR, Dabbs TP. J Mater Sci 1991;26:2313.
[37] Kurkjian CR, Kammlott GW, Chaudhri MM. J Am Ceram Soc 1995;78:737.
[38] Fabes BD, Uhlmann DR. J Am Ceram Soc 1990;73:978.
[39] Wang FH, Hand RJ, Ellis B, Seddon AB. Phys Chem Glasses 1995;36:201.
[40] Hill MJ, Rowcliffe DJ. J Mater Sci 1974;9:1569.
[41] Hockey BJ, Lawn BR. J Mater Sci 1975;10:1275.
[42] Lloyd SJ, Molina-Aldareguia JM, Clegg WJ. Philos Mag A 2002;82:1963.
[43] Pharr GM. Mater Sci Eng A 1998;253:151.